nature energy

ARTICLES

https://doi.org/10.1038/s41560-019-0448-5

Wide-gap non-fullerene acceptor enabling high-performance organic photovoltaic cells for indoor applications

Yong Cui[1,2], Yuming Wang[3], Jonas Bergqvist[3], Huifeng Yao[1], Ye Xu[1,2], Bowei Gao[1,2], Chenyi Yang[4], Shaoqing Zhang[4], Olle Inganäs[3], Feng Gao[3*] and Jianhui Hou[1,2,4*]

Organic photovoltaic cells are potential candidates to drive low power consumption off-grid electronics for indoor applications. However, their power conversion efficiency is still limited by relatively large losses in the open-circuit voltage and a non-optimal absorption spectrum for indoor illumination. Here, we carefully designed a non-fullerene acceptor named IO-4Cl and blend it with a polymer donor named PBDB-TF to obtain a photoactive layer whose absorption spectrum matches that of indoor light sources. The photovoltaic characterizations reveal a low energy loss below 0.60 eV. As a result, the organic photovoltaic cell (1 cm²) shows a power conversion efficiency of 26.1% with an open-circuit voltage of 1.10 V under a light-emitting diode illumination of 1,000 lux (2,700 K). We also fabricated a large-area cell (4 cm²) through the blade-coating method. Our cell shows an excellent stability, maintaining its initial photovoltaic performance under continuous illumination of the indoor light source for 1,000 hours.

With the advent of the internet of things, huge amounts of off-grid energy sources are needed for tens of billions of independent and electronic devices with a low power consumption for indoor applications[1–5]. Photovoltaic cells that can efficiently convert low-intensity light in the indoor environment into the megawatt to microwatt class of electrical power[6–10] are recognized as ideal candidates to drive the low power consumption devices. Emission spectra of the commonly used indoor light sources, such as fluorescent lamps and light-emitting diodes (LEDs), usually range from 400 to 700 nm (ref. [11]) with intensities less than 1 mW cm^{-2} (Supplementary Fig. 1)[12], which are spectrally much narrower with a weaker intensity than the standard solar spectrum (the global AM 1.5G spectrum) and, therefore, the photovoltaic cells developed to convert sunlight are not necessarily optimized for indoor applications. For example, the crystalline silicon cells show low power conversion efficiencies (PCEs) under indoor light[13,14]. On the contrary, although some of the emerging photovoltaic cells, such as organic photovoltaic (OPV) cells and dye-sensitized solar cells, are not as efficient as the crystalline silicon cells under standard solar illumination, the highly tunable light-absorption properties of their photoactive materials make them promising candidates for indoor applications[6,15–19]. Compared with dye-sensitized solar cells, OPV cells possess greater commercial prospects because of the advantages in a low-cost, large-area module by solution printing and coating techniques.

To obtain an excellent photovoltaic performance under the indoor light conditions, an OPV cell should have the following characteristics. First, it should have a photoresponse spectrum that matches the indoor light sources and a high external quantum efficiency (EQE) so as to efficiently convert the incident light into current as well as to minimize the thermalization of the photogenerated charges. Second, trap-mediated charge recombination must be effectively suppressed, as a low incident light intensity leads to a low carrier density, at which trap-mediated recombination becomes critical[20]. Third, energy loss ($E_{loss} = E_g - qV_{OC}$, where E_g is the bandgap, q is the elementary charge and V_{OC} is the open-circuit voltage) of the OPV cell should be as low as possible to maximize the V_{OC}. For OPV cells, energy losses less than 0.60 eV have been obtained under the standard AM 1.5G conditions[21–23]. In consideration of an extra voltage loss of ~0.2 V due to the significantly reduced light intensity[5], a V_{OC} of 1.0 V can be expected for an OPV cell with an E_g of 1.8 eV, a gap suitable for indoor applications. However, the V_{OC} values of state-of-the-art OPV cells are all below 0.8 V under the indoor light conditions[5,6,17,24,25], which significantly limits the PCEs. Therefore, to meet the requirements raised by indoor applications, more effort needs to be devoted to developing new OPV materials that can simultaneously offer a suitable absorption spectrum, low E_{loss} and minimized trap-mediated charge recombination.

In this work, we rationally designed and synthesized an acceptor–donor–acceptor (A-D-A)-structured small-molecule acceptor material named IO-4Cl (3,9-bis[5,6-dichloro-1*H*-indene-1,3(2*H*)-dione]-5,5,11,11-tetrakis(4-hexylphenyl)dithieno[2,3-*d*:2′,3′-*d*′]-*s*-indaceno[1,2-*b*:5,6-*b*&′rsquo;]dithiophene), which has an optical gap (E_g^{opt}) of 1.80 eV. By blending the acceptor with a polymer donor named PBDB-TF (poly[1-(5-(4,8-bis(5-(2-ethylhexyl)-4-fluorothiophen-2-yl)-6-methylbenzo[1,2-*b*:4,5-*b*′]dithiophen-2-yl) thiophen-2-yl)-5,7-bis(2-ethylhexyl)-3-(5-methylthiophen-2-yl)-4*H*,8*H*-benzo[1,2-*c*:4,5-*c*′]dithiophene-4,8-dione])[26], an OPV cell with an absorption band that ranges from 400 to 700 nm was fabricated. The PBDB-TF:IO-4Cl blend film shows an electroluminescence (EL) quantum efficiency (EQE_{EL}) of ~0.55×10^{-4}, which is

[1]State Key Laboratory of Polymer Physics and Chemistry, Beijing National Laboratory for Molecular Sciences, Institute of Chemistry, Chinese Academy of Sciences, Beijing, China. [2]School of Chemistry and Chemical Engineering, University of Chinese Academy of Sciences, Beijing, China. [3]Department of Physics, Chemistry and Biology, Linköping University, Linköping, Sweden. [4]School of Chemistry and Biology Engineering, University of Science and Technology Beijing, Beijing, China. *e-mail: feng.gao@liu.se; hjhzlz@iccas.ac.cn

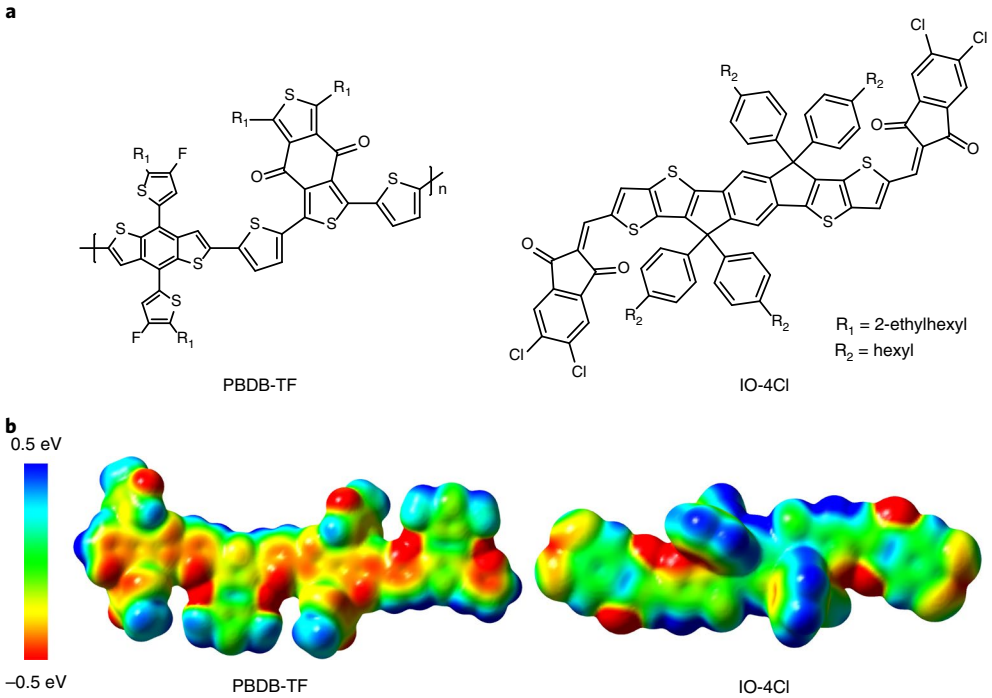

Fig. 1 | Molecular structures and ESP distributions of the materials. a, Molecular structures of PBDB-TF and IO-4Cl. **b**, ESP distributions from PBDB-TF and IO-4Cl. PBDB-TF has a negative ESP on the majority of its molecular surface. On the contrary, the conjugated backbone of IO-4Cl has a high average ESP. The difference of ESP is beneficial for the electron transfer from PBDB-TF to IO-4Cl.

among the highest values in OPV cells and indicates a low non-radiative recombination in the device. As a result, under the illumination of AM 1.5G (100 mW cm^{-2}), the OPV cell gives a PCE of 9.80% with a high V_{OC} of 1.24 V. Under the indoor light conditions simulated by a 2,700 K LED light (varied across 200–1,000 lux), the V_{OC} remains more than 1.00 V, which enables a high PCE. We also demonstrate that the OPV cell has great advantages in practical applications due to its excellent stability under indoor illumination conditions, insensitivity to series resistance and an active-layer thickness. As a consequence, a 4 cm^2 cell made by blade-coating exhibits a PCE of 23.9% with a thickness of 179 ± 38 nm under indoor illumination (2,700 K LED, 1,000 lux, 302.2 μW cm^{-2}), which provides a promising power source for many microelectronic devices.

Design and synthesis of the non-fullerene acceptor

The state-of-the-art non-fullerene acceptors with an A-D-A structure have shown promising photovoltaic properties, but their E_g^{opt} values are all too small to match the indoor light spectrum[27–30]. To blueshift the absorption spectrum and also maintain a high electrostatic potential (ESP) nature of the A-D-A acceptors, we designed an acceptor named IO-4Cl (Fig. 1a and Supplementary Figs. 2–4), a derivative of the representative A-D-A molecule ITIC[31]. As shown in Supplementary Fig. 5, the calculation results of a density functional theory (DFT) method demonstrate that IO-4Cl is expected to have a significantly blueshifted absorption spectrum and a similarly high electron-accepting capability compared with ITIC (Fig. 1b and Supplementary Fig. 6). We synthesized IO-4Cl by the approach given in Supplementary Note 1. As shown in Fig. 2a, the IO-4Cl film has an absorption band that covers the region from 450 to 700 nm, which is about 90 nm blueshifted compared with that of ITIC and corresponds to an E_g^{opt} of 1.80 eV. The lowest unoccupied molecular orbital (LUMO) and the highest occupied molecular orbital (HOMO) level of IO-4Cl were estimated to be −3.83 and −5.72 eV, respectively (Fig. 2b and Supplementary Fig. 8).

Device performance under AM 1.5G conditions

A large energy offset between the HOMO of the donor and the LUMO of the acceptor is required to obtain a high V_{OC} for OPV devices. We selected the polymer donor PBDB-TF with a low-lying HOMO of −5.41 eV and an E_g^{opt} of 1.80 eV (Fig. 2a,b) to blend with IO-4Cl to make 1 cm^2 OPV cells. The detailed photovoltaic parameters are listed in Supplementary Table 1. The current density–voltage (J–V) curve of a representative device is shown in Fig. 2c and Supplementary Fig. 9. For the optimal conditions (Supplementary Figs. 10 and 11), a PCE of 9.80% was achieved with a very high V_{OC} of 1.24 V, a short-circuit current (J_{SC}) of 11.6 mA cm^{-2} and a fill factor (FF) of 0.681. As displayed in Fig. 2d, the EQE spectrum of the device shows a photoresponse spectrum from 300 to 700 nm, which well meets the requirement for indoor applications. The corresponding integrated current density (J_{cal}) is 11.5 mA cm^{-2}. We also fabricated PBDB-TF-only and IO-4Cl-only devices, which show V_{OC} values of 1.26 and 1.27 V, respectively (Supplementary Fig. 12), which implies that V_{OC} of the PBDB-TF:IO-4Cl-based cell almost reaches the upper limit of the materials.

Several E_g definitions are used in the OPV community. To fairly compare the E_{loss} in our work with those reported in the literature, we defined the E_g from the derivative of the EQE edge[32–34]. The E_g of the PBDB-TF:IO-4Cl device is estimated to be 1.84 eV (Supplementary Fig. 13), and thus the E_{loss} in this device is 0.60 eV. Using the same method, we calculated the E_g and E_{loss} values for the OPV cells with the different photoresponse regions. As depicted in Fig. 3a (Supplementary Note 2), the cells with E_g above 1.8 eV usually show a relatively larger E_{loss} compared with those with smaller E_g. To understand why the PBDB-TF:IO-4Cl device shows an impressively small E_{loss}, we measured the EL and Fourier transform photocurrent spectroscopy EQE (FTPS-EQE) and then analysed the contributions of the radiative and non-radiative charge recombination to E_{loss} (refs [35,36]). E_{loss} is equal to the sum of three contributions: radiative recombination due to the absorption above the gap (ΔE_1), radiative recombination due to the absorption below the gap

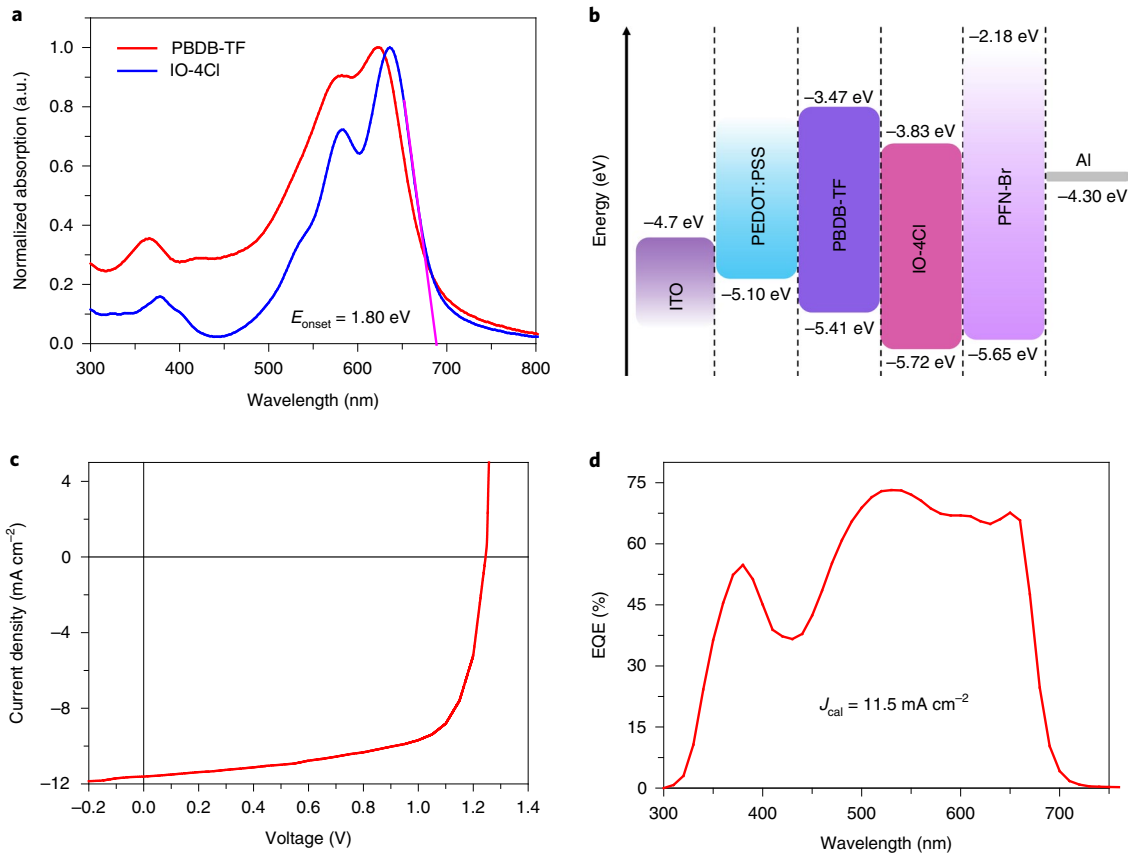

Fig. 2 | Absorption spectra and energy levels of the materials and their photovoltaic performances. a, Normalized ultraviolet–visible absorption spectra of PBDB-TF and IO-4Cl as films. The optical gap was determined by the intersection of the tangent (pink line) of the absorption spectrum and the abscissa axis. **b**, Molecular energy levels of the materials in this work. **c**, The *J*–*V* curve of a PBDB-TF:IO-4Cl-based OPV cell under AM1.5G conditions. **d**, The EQE curve of a PBDB-TF:IO-4Cl-based OPV cell. J_{cal} can be calculated by integrating the EQE curve over the photon flux spectrum under AM1.5G conditions. a.u., arbitrary units.

(ΔE_2) and non-radiative recombination (ΔE_3). ΔE_1 is unavoidable for any photovoltaic cell due to the thermodynamic limit, and it is a function of E_g at a given temperature (300 K in this work)[35]. As shown in Supplementary Fig. 14a, ΔE_1 increases with increasing E_g, which is one of the reasons that explains why the OPV cells with a large E_g usually display a relatively larger E_{loss}. We obtained a very small ΔE_2 of 0.07 eV, which benefits from the steep EQE tail (Fig. 3b)[37]. The EQE_{EL} of the device is as high as ~0.55×10^{-4}, which corresponds to a ΔE_3 of 0.25 eV (Fig. 3c), which is among the lowest values for OPV cells.

To understand the underlying mechanism of the high EQE_{EL} and thereby the low non-radiative recombination energy losses in our system, a comparison of the EL spectra of the donor, acceptor and blend is shown in Fig. 3d. The EL spectrum of the blend shows four emission peaks, located at 1.27, 1.47, 1.67 and 1.80 eV. The peak at 1.80 eV can be attributed to the emission of singlet states of the donor or acceptor by comparing the EL spectra. As the EL spectra of pure PBDB-TF and pure IO-4Cl both show weak vibronic peaks at 1.67 and 1.47 eV as well, these peaks may be associated with a vibronic progression coupled to the singlet of the donor, acceptor or both (Supplementary Fig. 14c,d). However, the peak at 1.47 eV is significantly enhanced in the blend. This might be due to the morphology change after blending[38,39] or to the resonance between the vibronic peaks of singlet excitons and the charge-transfer states. The emission of the blend has rich features, and a weak peak at 1.27 eV might also come from the vibronic progression. A solid explanation of all these emission peaks and their effect on the non-radiative recombination is beyond the scope of this work and requires further investigations.

Photovoltaic performance under indoor light conditions

We employed the commonly used fluorescent (2,700 K and 6,500 K) and LED (2,700 K and 6,500 K) lamps as light sources to simulate the indoor illumination environment; the photovoltaic results under the warm white LED lamp (2,700 K) are discussed in detail and the results under the other three lamps are provided in Supplementary Figs. 15 and 16 and Supplementary Table 2. In this work, the photovoltaic performance of the cell was investigated under 200, 500 and 1,000 lux, which represent the illumination conditions for typical indoor applications, such as the living room, library, supermarket and so on. For the 2,700 K LED lamp, the light power intensities at 200, 500 and 1,000 lux are 60.4, 151.1 and 302.2 μW cm^{-2}, respectively (Fig. 4a).

Figure 4b and Table 1 show the *J*–*V* curves and photovoltaic parameters of the cells at three illumination conditions. In Supplementary Fig. 17, the fitting of the dependence of J_{SC} on the light-intensity data yields a slope close to unity, which indicates that the ratio of photons to electrons remains constant with decreasing light intensity. Based on the EQE curve of the cell (Fig. 2d) and the incident photon flux spectrum (Fig. 4c), the integral current densities at the three illumination conditions, which are consistent with the values from *J*–*V* measurements, were calculated (listed in Table 1) and confirmed the reliability of our photovoltaic measurement (Supplementary Note 3). Under the three illumination conditions, PCEs that ranged from 22.2 to 26.1% were obtained. Note that the V_{OC} values are significantly higher than those of most of photovoltaic cells under the indoor light conditions[15–17], except for the GaAs-based cell[8]. In addition, we tested the stability of the cell under

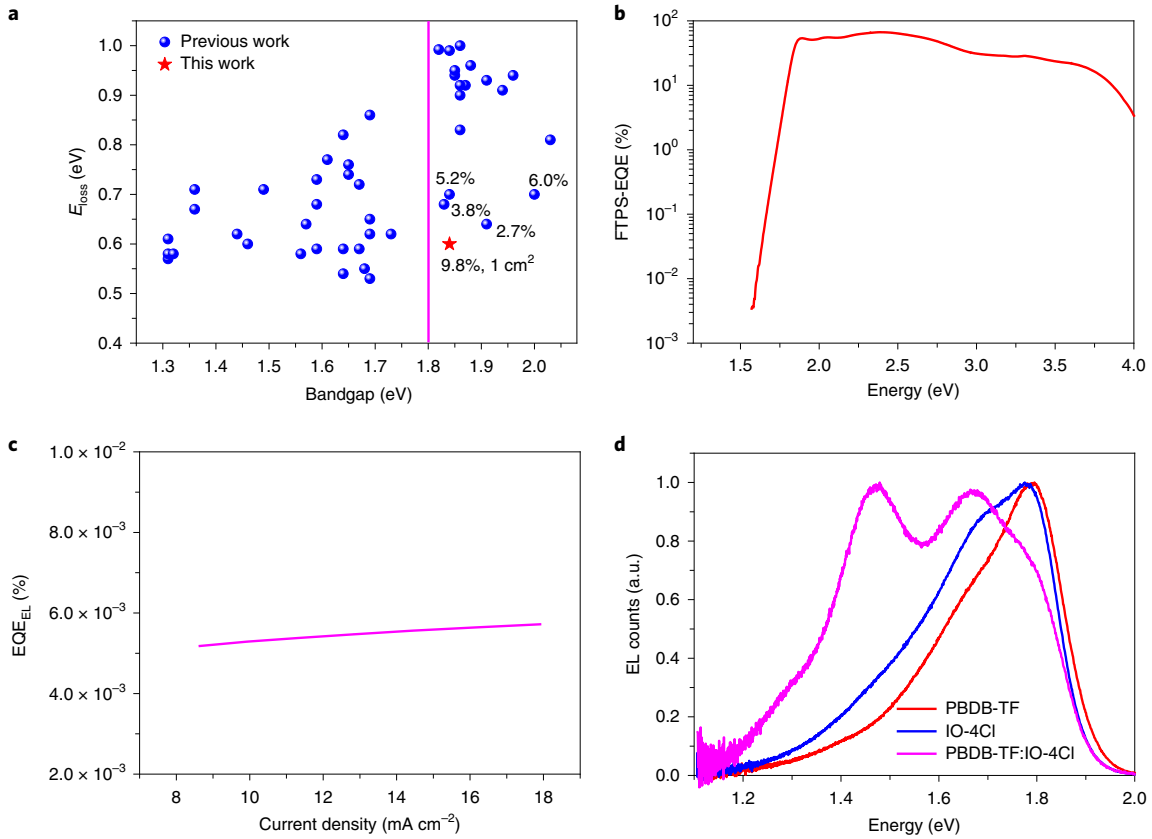

Fig. 3 | Energy losses of PBDB-TF:IO-4Cl-based cells. a, Plots of E_{loss} against E_g, which is determined from the derivative of the EQE edge. The values marked in this panel are PCEs. **b**, Normalized FTPS-EQE spectra of the PBDB-TF:IO-4Cl-based device. **c**, EQE_{EL} of PBDB-TF:IO-4Cl. **d**, Normalized EL spectra of neat PBDB-TF, neat IO-4Cl and blend PBDB-TF:IO-4Cl.

continuous illumination by the indoor light and, as shown in Fig. 4d, the cell almost maintained its initial PCE after 1,000 hours.

For comparison, we fabricated the 1 cm^2 cell based on the blend PBDB-TF:3,9-bis(5,6-difluoro-2-methylene-(3-(1,1-dicyanomethylene)-indanone)-5,5,11,11-tetrakis(4-hexylphenyl)-dithieno[2,3-d:2',3'-d']-s-indaceno[1,2-b:5,6-b']dithiophene (IT-4F), which exhibits a PCE of 12.5% under a solar simulation of AM 1.5G, and then characterized its photovoltaic performance under the illumination of a 2,700 K LED lamp at 1,000 lux. As shown in Supplementary Fig. 20 and Supplementary Table 3, this cell exhibits a PCE of 21.2%. Compared to the PBDB-TF:IO-4Cl-based cell under the same conditions, although J_{SC} of the PBDB-TF:IT-4F-based cell is 25% higher (114 versus 90.6 μA cm^{-2}) because of its relatively higher EQE, its V_{OC} is 35% lower (0.712 versus 1.10 V), which is the main cause of the relatively lower PCE. Therefore, the high V_{OC} of the PBDB-TF:IO-4Cl-based cell plays a critical role in realizing a high PCE under the indoor light conditions.

Large-area single cell

We then demonstrated the advantages of the OPV cells in making large-area devices for indoor applications. As is well known, OPV cells suffer a sharply increasing series resistance (R_s) caused by the transparent electrodes for large-area modules[40]. By introducing an external resistor in series (Fig. 5a), the PCE of the PBDB-TF:IO-4Cl-based cell sharply dropped by increasing the external R_s under one sun illumination. However, under indoor illumination, the PCE remained almost constant by adding a 1,000 Ω R_s and retained 65% of its initial value under the 10,000 Ω condition (Fig. 5a and Supplementary Fig. 21). Therefore, for indoor applications, the parasitic R_s caused by the transparent electrodes is not a limiting factor to the PCE and hence the shape of the large-area OPV cells does not have to be thin strips.

Another advantage with the OPV cells for indoor applications is that the performance is less dependent on the active-layer thickness, compared with the one sun conditions. A high tolerance to the active-layer thickness is more suitable for making large-area devices through printing techniques[41]. Figure 5b,c shows the variations of V_{OC}, J_{SC}, FF and PCE of the cells under the two illumination conditions, that is, the one sun and indoor conditions. In general, V_{OC} is determined by the split of the electron and hole quasi-Fermi energy levels[42]:

$$V_{OC} = 1/q(E_{Fn} - E_{Fp}) \quad (1)$$

where q is the elementary charge and E_{Fn} and E_{Fp} are the electron and hole quasi-Fermi levels, respectively, which are directly correlated with the density of states affected by light illumination[43,44]. Figure 5d shows a diagrammatic sketch of the density of states under strong and low illumination. With a decreasing incident light intensity along with the incident direction (Supplementary Fig. 22), the E_{Fn} shifts down and the E_{Fp} shifts up, which is the reason for the lower V_{OC} of the cells with the relatively thicker active layers, whether under the indoor light or one sun illumination.

Under the one sun conditions, the J_{SC} changes slightly and FF drops significantly with increasing thickness, consistent with previously reported results[45]. Under indoor illumination, the photogenerated carrier density is much lower than that under the one sun conditions, so the non-geminate charge recombination, in particular the bimolecular recombination, is reduced, which might be one of the reasons for the higher FF under the indoor illumination.

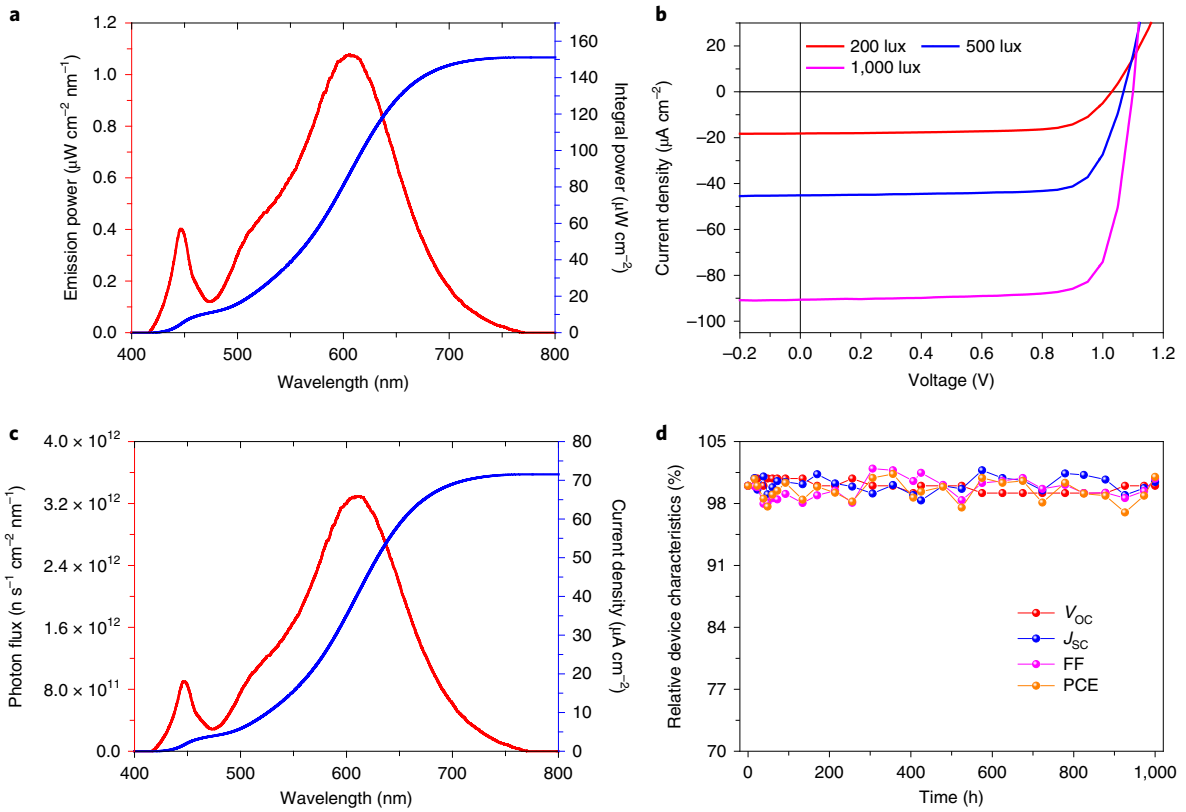

Fig. 4 | Photovoltaic performance for indoor applications. a, Emission power and integrated power spectra of the warm white 2,700 K LED at 500 lux. **b**, The *J*–*V* curves of the PBDB-TF:IO-4Cl-based optimal cell under different indoor light intensities. **c**, Photon flux and integrated current density spectra over the warm white 2,700 K LED 500 lux. **d**, The curves of the photovoltaic characteristics versus time. The curves are normalized to their initial values at the start of the lifetime test. The device was encapsulated and the testing was carried out at a temperature of 25–30 °C and a relative humidity of 40–60%. Single data points are connected with solid lines to display the trend.

Table 1 | Parameters of the OPV cells based on PBDB-TF:IO-4Cl under different light intensities under a 2,700 K LED lamp

Device	Light source (lux)	P_{in} (μW cm^{-2})	V_{OC} (V)	J_{SC} (μA cm^{-2})	FF	J_{cal} (μA cm^{-2})[a]	P_{out} (μW cm^{-2})	PCE (%)[b]
1 cm^2 device fabricated by a spin-coating method	200	60.4	1.03	18.2	0.715	17.9	13.4	22.2 (21.4 ± 0.5)
	500	151.1	1.07	45.1	0.768	44.7	37.1	24.6 (23.7 ± 0.5)
	1,000	302.2	1.10	90.6	0.791	89.3	78.8	26.1 (25.5 ± 0.4)
4 cm^2 device fabricated by a blade-coating method	200	60.4	1.02	18.3	0.743	17.5	13.9	23.0 (22.4 ± 0.3)
	500	151.1	1.05	45.0	0.748	43.7	35.3	23.4 (22.9 ± 0.3)
	1,000	302.2	1.07	89.5	0.753	87.4	72.1	23.9 (23.5 ± 0.3)

[a]J_{cal} was obtained by integrating the EQE spectrum over that of the light source. [b]The average parameters and s.d. were calculated from more than 20 independent cells. P_{in}, power in; P_{out}, power out.

According to the empirical expression for the FF of photovoltaic cells within the context of the equivalent circuit model[46,47], the dependence of the theoretical FF of the OPV cells under a very low J_{SC} on the incident light intensity can be obtained (Supplementary Note 5). As shown in Supplementary Table 1, compared to the 100 nm thick cell, the 300 nm thick cell possesses a fairly low FF under a high illumination, and the thicker cell shows a much higher FF when the light intensity is reduced (Supplementary Fig. 23). Therefore, under the indoor illumination conditions, although the V_{OC} of the thicker cell is slightly lower, its PCE is less sensitive to variation of the light intensity.

We also employed the blade-coating method to fabricate the photoactive layer and then made the large-area cell with a dimension of 2 × 2 cm^2. In consideration of preventing formation of pin-hole, which is detrimental to large area cells, the active layer was controlled to be 179 ± 38 nm. As shown in Fig. 5e, Supplementary Fig. 24 and Table 1 for the *J*-*V* curves and corresponding photovoltaic parameters of the cell, we obtained over 23% PCEs under the indoor illumination conditions. Interestingly, benefitting from the high FF feature, under the illumination at 200 lux, the PCE of this 4 cm^2 blade-coated cell still reaches 23.0%, which is even higher than the 1 cm^2 cell made by spin coating. In contrast, under the one sun condition, the 4 cm^2 cell only shows a PCE of 7.18% which is obviously lower than the 1 cm^2 cell (Supplementary Table 4).

Efficiency prediction for indoor applications

We predict the PCE potential of OPV cells for indoor applications with the following assumptions. The upper limit of J_{SC} is estimated

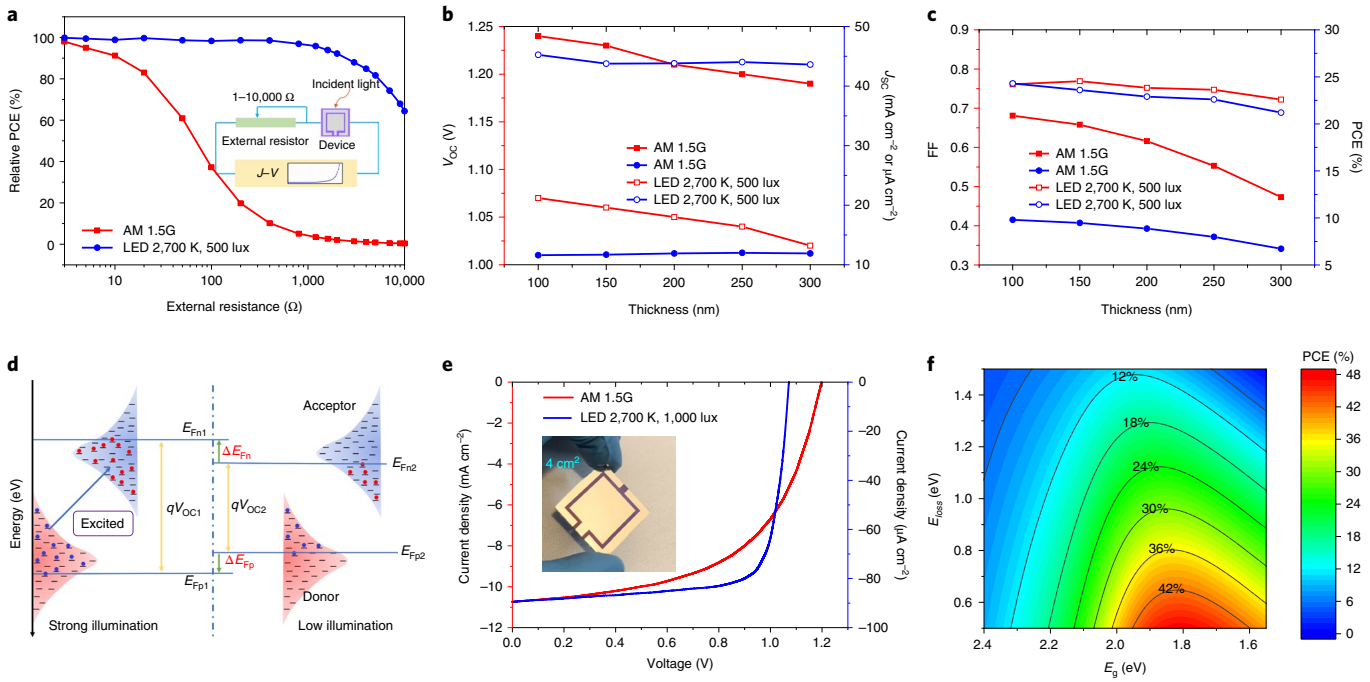

Fig. 5 | Photovoltaic performance of large-area devices. a, Dependence of PCEs on R_s at 500 lux and under AM1.5G conditions. Inset: schematic diagram of *J*–*V* measurement. **b**, V_{OC} and J_{SC} versus active-layer thickness plots at 500 lux and under AM1.5G conditions. **c**, FF and PCE versus active-layer thickness plots at 500 lux and under AM1.5G conditions. The single data points are connected with solid lines to display the trend. **d**, A diagram of the density of states in both the donor and acceptor materials under strong and low illumination. A detailed description of the diagram is given in Supplementary Note 4. Panel **d** adapted from Elumalai and Uddin[44], Royal Society of Chemistry. **e**, The *J*–*V* curves of a 4 cm^2 cell based on a blade-coating method under sunlight and an LED. Inset: digital photograph of the 4 cm^2 device fabricated via a blade-coating method. **f**, Efficiency prediction of the OPV cells for indoor applications (LED, 2,700 K). The colour scale indicates the PCEs of corresponding colours.

by assuming a step-function EQE of 90% above the gap, integrated over the emission spectrum of the indoor light. The V_{OC} is estimated by E_g and E_{loss}. Given the unavoidable ΔE_1 value of 0.25–0.35 eV and an additional loss of V_{OC} of about 0.15–0.20 V due to the significantly lower light intensity, we set the minimum value of E_{loss} to be 0.50 eV. As OPV cells can show a higher FF under weak light intensity, according to the empirical relationship reported in literature[46], the FF values shown in Supplementary Fig. 23a can be expected. Consequently, under the indoor light (2,700 K LED), an over 40% PCE can be expected, as shown in Fig. 5f.

Conclusion

We designed and synthesized an acceptor, IO-4Cl, with an E_g^{opt} of 1.80 eV. Blending IO-4Cl with a the polymer donor PBDB-TF, we fabricated an OPV cell with a large gap and low E_{loss}. Under the standard AM 1.5 G conditions, the 1 cm^2 OPV cell demonstrated a PCE of 9.80% with a V_{OC} of 1.24 V. Under the indoor illumination conditions, simulated by a 2,700 K LED lamp at 1,000 lux, the 1 cm^2 cell showed a PCE of 26.1% and maintained its initial photovoltaic performance under continuous illumination for 1,000 hours. More importantly, we demonstrated that under the indoor conditions, the PCE of the cell has a high tolerance to the parasitic resistance caused by a transparent electrode, and is not sensitive to thickness variation of the photoactive layer. These two features are of importance to future large-scale production and enabled us to successfully fabricate a 4 cm^2 cell through a blade-coating method, which showed an over 23% PCE under the indoor illumination at 200–1,000 lux.

Methods

Fabrication of the 1 cm^2 device via a spin-coating method. Devices were fabricated with the conventional device structure of glass/ITO/PEDOT:PSS/active layer/ poly(PFN-Br)/Al (ITO, indium tin oxide; PEDOT:PSS, poly(3,4-ethylenedioxythiophene) polystyrene sulfonate; PFN-Br, poly[(9,9-bis(3′-((*N*,*N*-dimethyl)-*N*-ethylammonium)-propyl)-2,7-fluorene)-alt-2,7-(9,9-dioctylfluorene)]). ITO-coated glass was purchased from South China Xiang's Science & Technical Company Limited and washed ultrasonically in water/detergent, water, acetone and isopropanol in sequence for 15 min. The corresponding resistance was 6 Ω cm^{-2}. For the anode interlayers, PEDOT:PSS (4083) was purchased from Clevios and diluted with the same volume of water. The polymer donor, PBDB-TF, was purchased from Solarmer Material Inc. (Lot PH906A). PBDB-TF:IO-4Cl (1:1.5) was dissolved in chlorobenzene at a polymer concentration of 10 mg ml^{-1}. To dissolve the polymers fully, the active-layer solution PBDB-TF:IO-4Cl was stirred at 40 °C for 4 h. For the cathode interlayer, PFN-Br was purchased from Solarmer Material Inc. and dissolved in methanol to give a concentration of 0.5 mg ml^{-1}. Devices were fabricated as follows. First, the ITO-coated glass substrates were treated in ultraviolet–ozone for 20 min. About a 10 nm PEDOT:PSS layer was spin coated on the ITO substrates and annealed at 150 °C for 20 min. Subsequently, the substrates were transferred to a glove box. The active-layer solutions were spin coated onto the PEDOT:PSS, and the films were treated with thermal annealing at 160 °C for 10 min. The thickness of all the active layers was about 100 nm. The PFN-Br layer was spin coated on top of the active layer at 3,000 r.p.m. for 30 s. Finally, a 100 nm Al layer was deposited under high vacuum (~3 × 10^{-4} Pa).

Fabrication of the 4 cm^2 device via a blade-coating method. The fabrication process for the blade-coated device was the same as that for the spin-coated device. The difference was in the preparation of the active layer. For the blade-coated device, PBDB-TF:IO-4Cl (1:1.5) was dissolved in chlorobenzene at a polymer concentration of 3.8 mg ml^{-1}. Before blade coating, ITO-coated glasses were preheated on a hot plate at 70 °C. When coating the active layer, the blade moved at a speed of 5 cm s^{-1}.

Device characterization and measurement. The *J*–*V* measurement was performed via the solar simulator (SS-F5-3A, Enlitech) along with AM 1.5G spectra whose intensity was calibrated by a certified standard silicon solar cell (SRC-2020, Enlitech) at 100 mW cm^{-2}. The AM 1.5G light source with a spectral mismatch factor of 1.01 was calibrated by the National Institute of Metrology. The intensity of the AM 1.5G spectra was calibrated by a certified standard silicon solar cell (SRC-2020, Enlitech) calibrated by the National Institute of Metrology. The emission spectra and illumination intensities of the light sources were measured

by a high-precision fibre-optics spectrometer (Maya2000 Pro, Ocean Optics). *J*–*V* curves were measured in the forward direction from −0.2 to 1.5 V, with a scan step of 50 mV and a dwell time of 5 ms. The area of the tested solar cells was determined by an optical microscope. The effective areas of the cells were 1.071 cm^2 and 3.917 cm^2, respectively. The 1 cm^2 OPV cell was measured by the aperture (0.994 cm^2). The cells were characterized under a temperature of 25–30 °C in a glove box filled with nitrogen. The photovoltaic characteristics were measured independently at the Institute of Chemistry, Chinese Academy of Sciences and Linköping University. To investigate the dependence of the device performance on the light intensity, neutral density filters were used to tune the light intensity, which was calibrated by a standard Si solar cell. The EQE spectrum was measured through the Solar Cell Spectral Response Measurement System QE-R3011 (Enli Technology Co., Ltd). The EQE_{EL} values were obtained from an in-house-built system that comprised a Hamamatsu silicon photodiode 1010B, a Keithley 2400 SourceMeter to supply the voltages and record the injected currents and a Keithley 485 picoammeter to measure the emitted light intensity. FTPS-EQE was measured using a Vertex 70 from Bruker Optics, equipped with a quartz tungsten halogen lamp, quartz beam-splitter and an external detector option. A low-noise current amplifier (SR570) was used to amplify the photocurrent produced on illumination of the photovoltaic devices with light modulated by the Fourier transform infrared spectroscope (FTIR). The output voltage of the current amplifier was fed back into the external detector port of the FTIR, to be able to use the FTIR's software to collect the photocurrent spectrum. Photoinduced charge extraction by linearly increasing the voltage measurement reported was performed by the all-in-one characterization platform Paios developed and commercialized by Fluxim AG. To reflect the true information, all the devices are prepared according to the corresponding device fabrication conditions.

Materials characterization. The ultraviolet–visible absorption spectroscopy measurements were conducted on a Hitachi UH4150 spectrophotometer. The energy levels (HOMO and LUMO) of the materials were measured by electrochemical cyclic voltammetry on a CHI650D electrochemical workstation with a three-electrode system. The cyclic voltammetry measurement used Pt wire as the counter electrode, a glassy carbon electrode as the working electrode, Ag/Ag^+ as the reference electrode and the ferrocene/ferrocenium redox couple as the internal calibration in a 0.1 M Bu_4NPF_6 acetonitrile solution at a scan rate of 50 mV s^{-1}. All the calculations were performed with Gaussian09. The optimal geometries, dipole moment and HOMO/LUMO energy levels were all calculated by DFT at the B3LYP/6–31G(d,p) level. The electron density isosurfaces were set to 0.001 atomic units when calculating the ESPs. Time-dependent DFT at the B3LYP/6-31G(d,p) level was used to simulate the ultraviolet–visible spectrum. Atomic force microscopy measurements were performed on a Vecoo Nanoscope IIIa using the tapping mode.

Reporting summary. Further information on research design is available in the Nature Research Reporting Summary linked to this article.

Data availability

The data that support the plots within this paper and other findings of this study are available from the corresponding author upon reasonable request.

Received: 10 September 2018; Accepted: 11 July 2019;
Published online: 19 August 2019

References

1. Atzori, L., Iera, A. & Morabito, G. The internet of things: a survey. *Comput. Netw.* **54**, 2787–2805 (2010).
2. Gubbi, J., Buyya, R., Marusic, S. & Palaniswami, M. Internet of things (IoT): a vision, architectural elements, and future directions. *Future Gener. Comp. Syst.* **29**, 1645–1660 (2013).
3. Al-Fuqaha, A., Guizani, M., Mohammadi, M., Aledhari, M. & Ayyash, M. Internet of things: a survey on enabling technologies, protocols, and applications. *IEEE Commun. Surv. Tut.* **17**, 2347–2376 (2015).
4. Khan, J. A., Qureshi, H. K. & Iqbal, A. Energy management in wireless sensor networks: a survey. *Comput. Electr. Eng.* **41**, 159–176 (2015).
5. Yin, H. et al. Designing a ternary photovoltaic cell for indoor light harvesting with a power conversion efficiency exceeding 20%. *J. Mater. Chem. A* **6**, 8579–8585 (2018).
6. Lee, H. K. H., Li, Z., Durrant, J. R. & Tsoi, W. C. Is organic photovoltaics promising for indoor applications? *Appl. Phys. Lett.* **108**, 253301 (2016).
7. Minnaert, B. & Veelaert, P. A proposal for typical artificial light sources for the characterization of indoor photovoltaic applications. *Energies* **7**, 1500–1516 (2014).
8. Freitag, M. et al. Dye-sensitized solar cells for efficient power generation under ambient lighting. *Nat. Photon.* **11**, 372–378 (2017).
9. Teran, A. S. et al. Energy harvesting for GaAs photovoltaics under low-flux indoor lighting conditions. *IEEE Trans. Electron. Dev.* **63**, 2820–2825 (2016).
10. Freunek, M., Freunek, M. & Reindl, L. M. Maximum efficiencies of indoor photovoltaic devices. *IEEE J. Photovolt.* **3**, 59–64 (2013).
11. Minnaert, B. & Veelaert, P. Efficiency simulations of thin film chalcogenide photovoltaic cells for different indoor lighting conditions. *Thin Solid Films* **519**, 7537–7540 (2011).
12. Mori, S. et al. Investigation of the organic solar cell characteristics for indoor LED light applications. *Jpn J. Appl. Phys.* **54**, 071602 (2015).
13. De Rossi, F., Pontecorvo, T. & Brown, T. M. Characterization of photovoltaic devices for indoor light harvesting and customization of flexible dye solar cells to deliver superior efficiency under artificial lighting. *Appl. Energy* **156**, 413–422 (2015).
14. Cutting, C. L., Bag, M. & Venkataraman, D. Indoor light recycling: a new home for organic photovoltaics. *J. Mater. Chem. C* **4**, 10367–10370 (2016).
15. Cao, Y., Liu, Y., Zakeeruddin, S. M., Hagfeldt, A. & Grätzel, M. Direct contact of selective charge extraction layers enables high-efficiency molecular photovoltaics. *Joule* **2**, 1108–1117 (2018).
16. Li, M. et al. Interface modification by ionic liquid: a promising candidate for indoor light harvesting and stability improvement of planar perovskite solar cells. *Adv. Energy Mater.* **8**, 1801509 (2018).
17. Lee, H. K. H. et al. Organic photovoltaic cells—promising indoor light harvesters for self-sustainable electronics. *J. Mater. Chem. A* **6**, 5618–5626 (2018).
18. Liu, X., Huettner, S., Rong, Z., Sommer, M. & Friend, R. H. Solvent additive control of morphology and crystallization in semiconducting polymer blends. *Adv. Mater.* **24**, 669–674 (2012).
19. Lin, Y. Z. & Zhan, X. W. Non-fullerene acceptors for organic photovoltaics: an emerging horizon. *Mater. Horiz.* **1**, 470–488 (2014).
20. Gupta, V. et al. Barium: an efficient cathode layer for bulk-heterojunction solar cells. *Sci. Rep.* **3**, 1965 (2013).
21. Zhang, H. et al. Fullerene-free polymer solar cell based on a polythiophene derivative with an unprecedented energy loss of less than 0.5 eV. *J. Mater. Chem. A* **4**, 18043–18049 (2016).
22. Xu, X. et al. Realizing over 13% efficiency in green-solvent-processed nonfullerene organic solar cells enabled by 1,3,4-thiadiazole-based wide-bandgap copolymers. *Adv. Mater.* **30**, 1703973 (2018).
23. Zhang, J., Tan, H. S., Guo, X., Facchetti, A. & Yan, H. Material insights and challenges for non-fullerene organic solar cells based on small molecular acceptors. *Nat. Energy* **3**, 720–731 (2018).
24. Aoki, Y. Photovoltaic performance of organic photovoltaics for indoor energy harvester. *Org. Electron.* **48**, 194–197 (2017).
25. Lechêne, B. P. et al. Organic solar cells and fully printed super-capacitors optimized for indoor light energy harvesting. *Nano Energy* **26**, 631–640 (2016).
26. Zhang, M., Guo, X., Ma, W., Ade, H. & Hou, J. A large-bandgap conjugated polymer for versatile photovoltaic applications with high performance. *Adv. Mater.* **27**, 4655–4660 (2015).
27. Zhang, H. et al. Over 14% efficiency in organic solar cells enabled by chlorinated nonfullerene small-molecule acceptors. *Adv. Mater.* **30**, 1800613 (2018).
28. Zhang, S., Qin, Y., Zhu, J. & Hou, J. Over 14% efficiency in polymer solar cells enabled by a chlorinated polymer donor. *Adv. Mater.* **30**, 1800868 (2018).
29. Zhao, F. et al. Single-junction binary-blend nonfullerene polymer solar cells with 12.1% efficiency. *Adv. Mater.* **29**, 1700144 (2017).
30. Lin, Y. et al. Mapping polymer donors toward high-efficiency fullerene free organic solar cells. *Adv. Mater.* **29**, 1604155 (2017).
31. Lin, Y. et al. An electron acceptor challenging fullerenes for efficient polymer solar cells. *Adv. Mater.* **27**, 1170–1174 (2015).
32. Nikolis, V. C. et al. Reducing voltage losses in cascade organic solar cells while maintaining high external quantum efficiencies. *Adv. Energy Mater.* **7**, 1700855 (2017).
33. Vandewal, K., Benduhn, J. & Nikolis, V. C. How to determine optical gaps and voltage losses in organic photovoltaic materials. *Sustain. Energy Fuels* **2**, 538–544 (2018).
34. Wang, Y. et al. Optical gaps of organic solar cells as a reference for comparing voltage losses. *Adv. Energy Mater.* **8**, 1801509 (2018).
35. Yao, J. et al. Quantifying losses in open-circuit voltage in solution-processable solar cells. *Phys. Rev. Appl.* **4**, 014020 (2015).
36. Liu, J. et al. Fast charge separation in a non-fullerene organic solar cell with a small driving force. *Nat. Energy* **1**, 16089 (2016).
37. Qian, D. et al. Design rules for minimizing voltage losses in high-efficiency organic solar cells. *Nat. Mater.* **17**, 703–709 (2018).
38. Ran, N. A. et al. Harvesting the full potential of photons with organic solar cells. *Adv. Mater.* **28**, 1482–1488 (2016).
39. Li, W. et al. Molecular order control of non-fullerene acceptors for high-efficiency polymer solar cells. *Joule* **3**, 1–15 (2018).
40. Zhang, J. et al. Enhancing performance of large-area organic solar cells with thick film via ternary strategy. *Small* **13**, 1700388 (2017).

41. Zhang, K. et al. Efficient large area organic solar cells processed by blade-coating with single-component green solvent. *Solar RRL* **2**, 1700169 (2018).
42. Vandewal, K., Tvingstedt, K., Gadisa, A., Inganas, O. & Manca, J. V. On the origin of the open-circuit voltage of polymer–fullerene solar cells. *Nat. Mater.* **8**, 904–909 (2009).
43. Cowan, S. R., Roy, A. & Heeger, A. J. Recombination in polymer–fullerene bulk heterojunction solar cells. *Phys. Rev. B* **82**, 245207 (2010).
44. Elumalai, N. K. & Uddin, A. Open circuit voltage of organic solar cells: an in-depth review. *Energy Environ. Sci.* **9**, 391–410 (2016).
45. Guo, B. et al. High efficiency nonfullerene polymer solar cells with thick active layer and large area. *Adv. Mater.* **29**, 1702291 (2017).
46. Green, M. A. Solar-cell fill factors—general graph and empirical expressions. *Solid State Electron.* **24**, 788–789 (1981).
47. Zhou, Y. H. et al. All-plastic solar cells with a high photovoltaic dynamic range. *J. Mater. Chem. A* **2**, 3492–3497 (2014).

Acknowledgements

The authors acknowledge financial support from National Natural Science Foundation of China (Grant nos. 51673201 and 91633301), Beijing National 434 Laboratory for Molecular Sciences (Grant no. BNLMS-CXXM-201903), Chinese Academy of Sciences (Grant no. XDB12030200), the Swedish Research Council VR (2018-06048), the Swedish Energy Agency Energimyndigheten (2016-010174) and the Swedish Government Strategic Research Area in Materials Science on Functional Materials at Linköping University (Faculty Grant no. SFO-Mat-LiU #2009-00971). F.G. is a Wallenberg Academy Fellow and O.I. is a Wallenberg Academy Scholar.

Author contributions

Y.C. and J.H. designed the experiments. Y.C. synthesized the acceptor material IO-4Cl. Y.C. fabricated the solar cells and carried out the published device performance measurements. F.G. led the work at Linköping. J.B. initiated the indoor characterization, performed the first indoor device measurements and contributed to the design of the indoor measurements. Y.W. measured the FTPS-EQE and EQE_{EL}. Y.X. performed the DFT calculations. B.G. carried out photo-CELIV (charge extraction by linearly increasing voltage) measurements. C.Y. provided atomic force microscopy images. O.I. contributed to the data interpretation. S.Z. analysed the dependence of the PCEs on R_s under the indoor and AM 1.5G conditions. Y.C., H.Y., F.G. and J.H. wrote the paper. All the authors discussed the results and commented on the manuscript.

Competing interests

J.B. and O.I. are co-founders of the company Epishine AB focused on commercializing OPV for indoor applications.

Additional information

Supplementary information is available for this paper at https://doi.org/10.1038/s41560-019-0448-5.

Reprints and permissions information is available at www.nature.com/reprints.

Correspondence and requests for materials should be addressed to F.G. or J.H.

Publisher's note: Springer Nature remains neutral with regard to jurisdictional claims in published maps and institutional affiliations.

nature research

Corresponding author(s): Jianhui Hou; Feng Gao

Solar Cells Reporting Summary

Nature Research wishes to improve the reproducibility of the work that we publish. This form is intended for publication with all accepted papers reporting the characterization of photovoltaic devices and provides structure for consistency and transparency in reporting. Some list items might not apply to an individual manuscript, but all fields must be completed for clarity.

For further information on Nature Research policies, including our data availability policy, see Authors & Referees.

Experimental design

Please check: are the following details reported in the manuscript?

1. Dimensions

Area of the tested solar cells	☒ Yes ☐ No	Area of the tested solar cells is provided in methods, section"Device characterization and measurement"
Method used to determine the device area	☒ Yes ☐ No	The method is provided in methods, section"Device characterization and measurement"

2. Current-voltage characterization

Current density-voltage (J-V) plots in both forward and backward direction	☐ Yes ☒ No	Just J-V plot in forward direction since there is no hysteresis in organic solar cell.
Voltage scan conditions *For instance: scan direction, speed, dwell times*	☒ Yes ☐ No	The scan conditions are provided in methods, section"Device characterization and measurement"
Test environment *For instance: characterization temperature, in air or in glove box*	☒ Yes ☐ No	Test environment is provided in methods, section"Device characterization and measurement"
Protocol for preconditioning of the device before its characterization	☐ Yes ☒ No	No preconditioning protocol.
Stability of the J-V characteristic *Verified with time evolution of the maximum power point or with the photocurrent at maximum power point; see ref. 7 for details.*	☐ Yes ☒ No	we only tested the long-term stability.

3. Hysteresis or any other unusual behaviour

Description of the unusual behaviour observed during the characterization	☐ Yes ☒ No	No. In general, organic solar cells do not have hystereisis problems.
Related experimental data	☐ Yes ☒ No	NO.

4. Efficiency

External quantum efficiency (EQE) or incident photons to current efficiency (IPCE)	☒ Yes ☐ No	EQE curve is shown in Figure 2d
A comparison between the integrated response under the standard reference spectrum and the response measure under the simulator	☒ Yes ☐ No	The comparison is provided in methods, section"Device characterization and measurement"
For tandem solar cells, the bias illumination and bias voltage used for each subcell	☐ Yes ☒ No	Our cells were only fabricated for single solar cells.

5. Calibration

Light source and reference cell or sensor used for the characterization	☒ Yes ☐ No	Relative information is provided in methods, section"Device characterization and measurement"
Confirmation that the reference cell was calibrated and certified	☒ Yes ☐ No	Relative information is provided in methods, section"Device characterization and measurement"

Calculation of spectral mismatch between the reference cell and the devices under test	☐ Yes ☒ No	There is no reference cell for measuring the emission intensity of the indoor light source, so we measured the light intensity by a luminescence efficiency measurement system. This part of information is provided in methods section "Instruments and Measurement".

6. Mask/aperture

Size of the mask/aperture used during testing	☒ Yes ☐ No	Size of the mask is provided in methods, section"Device characterization and measurement"
Variation of the measured short-circuit current density with the mask/aperture area	☐ Yes ☒ No	Our cells were only measured by the mask with 0.994 cm2 area.

7. Performance certification

Identity of the independent certification laboratory that confirmed the photovoltaic performance	☐ Yes ☒ No	There are not the independent certification laboratory for indoor application. But, the device performance was measured independently in Beijing and Linköping.
A copy of any certificate(s) *Provide in Supplementary Information*	☐ Yes ☒ No	There are not the independent certification laboratory for indoor application.

8. Statistics

Number of solar cells tested	☒ Yes ☐ No	Number of solar cells tested is provided in Table 1.
Statistical analysis of the device performance	☒ Yes ☐ No	Statistical results of the devices are listed in Table 1.

9. Long-term stability analysis

Type of analysis, bias conditions and environmental conditions *For instance: illumination type, temperature, atmosphere humidity, encapsulation method, preconditioning temperature*	☒ Yes ☐ No	Long-term stability analysis can be found in the section “Photovoltaic performance under indoor light conditions”